TITLE
AUTHORS
DATE

Abstract

Contents

1 Introduction

The standard model (SM) of particle physics is very successful at describing the fundamental constituents of matter in our universe. Through experiments with particle accelerators, many of the theoretical details in the SM has been corroborated. To further test the theory larger accelerators are needed, which led to the construction of the large hadron collider (LHC), finished in 2008. Particles are collided together at high energy to probe the properties of the produced debris, hoping to discover new physics that deviates from the SM.

The top quark was discovered in 1995, by experiments done by CDF[2] and DØ[1]. It is the heaviest known fundamental particle, with a mass of $173.34 \pm 0.27 \pm 0.71 \mathrm{GeV/c^2}$, and its coupling strength to all the bosons are well predicted by the standard model. Because of its heavy mass and consequently short lifetime, it doesn't have enough time to bind with lighter quarks and form hadrons before it decays, which means that it effectively decays, to a good approximation, as a free quark. Measurements of the top quark's properties plays an important role in testing the Standard Model. Top quark production at LHC occurs via strong interactions, where they are produced in top, anti-top pairs. One test of the Standard Model, is the study of the Wtb vertex Lorentz structure and coupling, which is studied by looking at the decay products of top quarks. The top quarks decay, with almost 100% branching fraction, by weak interactions into W bosons and bottom quarks $t \to W + b$. The W bosons decay, into either a charged lepton and neutrino; $W \to l + \nu_l$, or into a quark, anti-quark pair: $W \to q' + \bar{q}$.

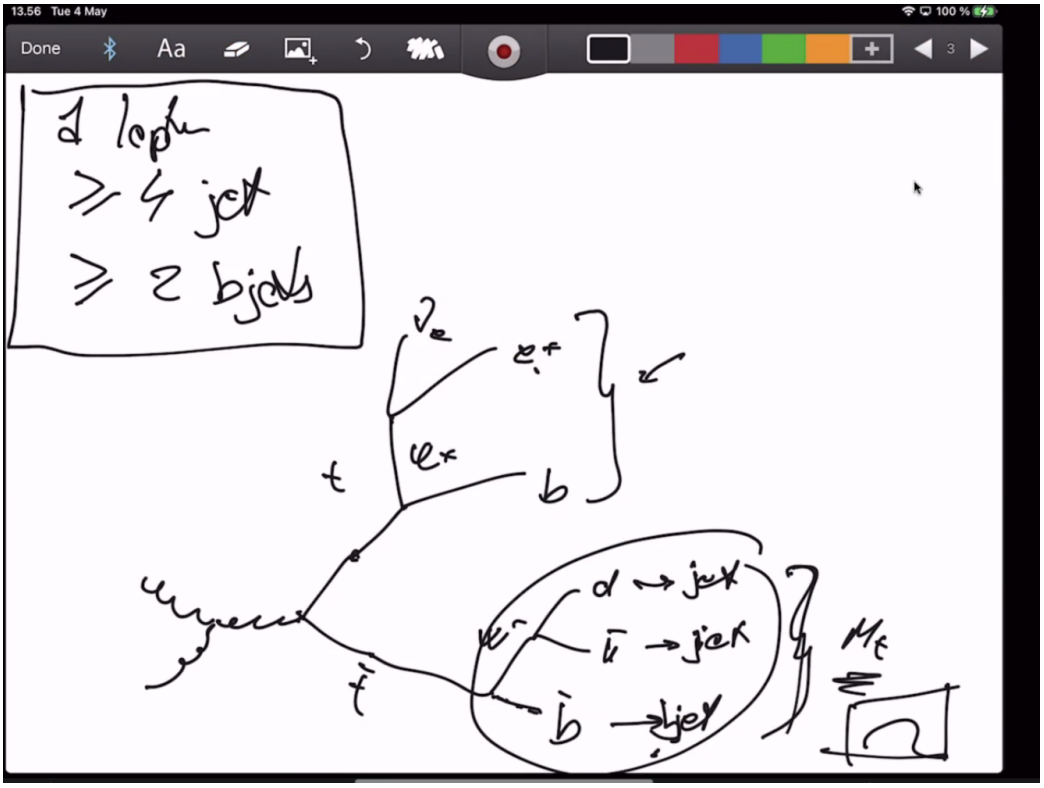

Figure 1: The Feynman diagram shows one of the possible decays of the top quarks. For this single leptonic decay, we see from the figure that there are 4 quark jets as the end product.

In this report, we are only looking at decays with a single lepton as decay product. The leptons we look at are either electrons or muons, and the collision will produce four jets, as evident from the diagram.

2 Theory

2.1 Standard Model

The Standard Model is a relativistic quantum field theory that describes three of the four fundamental forces, (the electromagnetic force, the strong force and the weak force), into a single theoretical framework. It contains all the known elementary particles, and how these particles interact with the different fields. The standard model manages to unify the electromagnetic (EM), and the weak force into different aspects of the same force called the electroweak force, while describing strong interactions through the frame-

work of Quantum Chromodynamics.

The elementary particles can be split into two distinct categories, called fermions and bosons. Fermions are defined by their spin, which is a half odd integer spin, but is exclusively 1/2 for all the elementary fermions of the Standard Model. They obey the pauli-exclusion principle which means that two identical fermions can't occupy the same quantum state. The fermions are grouped into quarks and leptons, each with three generations or families based on their masses. All of the fermions have an antiparticle associated with them, each with opposite charge, and apart from these antiparticle partners, there are a total of twelve known fermions, two leptons and two quarks in each family. The quarks that pair together in each generation are; the up and down quark, the charm and strange quark, and the top and bottom quark. The leptons, electron, muon and tau, each pair together with a neutrally charged neutrino.

In the SM, the fermions interact via gauge bosons, integer spin particles, which include the photon, gluon, W- and Z-boson, also called force carrier particles of the: electromagnetic force, the strong force and the weak force respectively. Quarks interact with the EM and the strong force, while leptons interact only with the electroweak force. Because neutrinos are neutrally charged, they will only interact via the weak force. Several unique features is found in weak interactions, such as parity violation (P), violation of charge conjugation (C), as well as a violation of the combined charge conjugation and parity symmetry (CP). Weak interactions does obey the combination of charge conjugation, parity, and time reversal symmetry.

2.1.1 Quantum Chromodynamics

Quantum chromo dynamics (QCD), is the theory of the strong interaction, which binds the quarks together. In the year 1964, physicist Murray Gell-Mann and his PhD student George Zweig, proposed that baryons and mesons could be explained by the existence of smaller triplet particles[7]. Since the Pauli exclusion principle forbids any fermions from inhabiting the same state, leading to the development of the concept of color in 1973[6] by phycisists Harald Fritzsh, Heinrich Leutwyler and Murray Gell-mann, suggesting that these quarks had additional conserved quantum numbers, later named color charge.

In QCD, each quark is associated with a color charge that confines the quark via the strong interaction to other quarks to make up a total color

charge that is neutral. While the color charge isn't physically related to actual colors, the way they mix together, is analogous to the way we mix the colors green, red and blue, as well as their anti colors, magenta, yellow and cyan. Because of these properties, quarks can bind together in groups with odd number of quarks with at least three to form baryons, or an even number of at least two to form mesons.

If enough energy is added to stretch one of the quarks away from the rest, the gluon field breaks, and a new quark and anti quark pair is created. This process of creating new quark, anti quark pairs, by stretching the gluon field between them is the result of violent inelastic collisions, which creates these jets of quarks, anti quarks.

2.1.2 Symmetries and Laws of Conservation

In the year 1971, Emmy Noether showed that any conservation law is associated with a continues symmetry of the Lagrangian[9]. The conservation laws of classical physics are the result of them being invariant with respect to their canonically conjugate quantities. The conservation of energy, linear momentum and angular momentum, stems from their invariance in time, space and angles respectively. This implies that the laws of physics are independent of the time, the location and the orientation in space.

Another symmetry, that is very important for quantum mechanics, is the reflection symmetry, called parity. A wave function can have positive or negative parity depending on whether or not it changes sign under parity transformation. For the laws which are invariant under reflection in space, the parity quantum number P is conserved, while in relativistic quantum mechanic, we need to ascribe an intrinsic parity to particles and antiparticles.

Group theory gives the tools to study these symmetries more elegantly, and has become particularly useful to describe symmetries of quantum mechanics, where degenerate eigenstates furnishes irreducible representations of a group. In studying these groups, we can discover other conserved quantities in the interactions of the EM, the weak or the strong force.

The unitary group U(1), leads to conservation of charge in EM and strong interactions, as well as the conservation of lepton number, as far as we know in all interactions. Certain particles behave practically identically with respect to the strong or the weak interactions, these properties are studied

through irreducible representations of the group SU(3), and are characterized by strong and weak isospin, which are also conserved.

The Dirac equation extends the Schrödinger wave equations, to include the effects of special relativity. The solution to this equation shows that for relativistic particles, where $\beta = v/c \to 1$, the projection of a particle's spin onto the direction of their momentum is conserved. This conserved quantity is called helicity[11, p. 63] and is defined as

$$h = \frac{\mathbf{s} \cdot \mathbf{p}}{|\mathbf{s}| \cdot |\mathbf{p}|}, \tag{1}$$

where $\mathbf{s}$ is the spin, and $\mathbf{p}$ is the momentum of the particle. For spin 1 particles, the Gauge bosons, the particle can take on three distinct helicity values, $h = -1$, $h = 0$ and $h = 1$, which corresponds to left handed, longtitudinal and right handed respectively.

Chirality is a fundamental property of a particle determined by representation theory. In the relativistic limit the distinction between helicity and chirality disappears, as the mass term mc^2 becomes negligible compared to the total energy. The weak force will only interact with left-chiral particles and right-chiral antiparticles. The operator of an interaction that describes the exchange of a boson, can have both vector V and axial vector A nature. If it has both a vector and an axial part, as in the case of weak interactions, parity is violated, while maximum parity violation occurs when both the contributions becomes equal magnitude.

After the discovery of parity violation and charge conjugation, by physicist C.S Wu[13], it was believed by physicists that CP-symmetry, the combination of charge conjugation symmetry and parity, was a true symmetry of the Standard model, until that too was violated in weak decay of neutral kaons, forcing physicists to reformulate the electroweak interaction in the Standard Model. The Cabbibo-Kobayashi-Maskawa (CKM) matrix explains how the flavour eigenstates of the quarks are related to the mass eigenstates, and is a 3×3 unitary matrix, with four independant parameters: three real angles and an imaginary phase[11, p. 153]. The imaginary phase gives rise to CP violation, but the matrix preserves CPT symmetry.

2.2 Four-momentum

The data collected in LHC collisions, allows us to reconstruct the 4-vector of momentum for the involved particles. This 4-vector is a four component

tensor, made up of an ordinary 3-vector for relativistic momentum $\mathbf{p}$, and the relativistic energy term, E^2/c^2, as its first component. Working in natural units, where we set $c = 1$, our 4-vector will be given as

$$p = \begin{pmatrix} E^2 \\ \mathbf{p} \end{pmatrix}. \tag{2}$$

The dot product of two 4-vectors is given by $p \cdot p' = EE' - \mathbf{p} \cdot \mathbf{p}'$, where $\mathbf{p} \cdot \mathbf{p}'$ is the ordinary dot product of two 3-vector momentum. From special relativity, we know that $E^2 - |\mathbf{p}|^2 = m^2$, so from the dot product, we get that $p^2 = m^2$. Other vector operations on a 4-vector is similar to those same vector operations on a 3-vector. The quantity

$$s = (p + p')^2 = (E + E')^2 - (\mathbf{p} + \mathbf{p}')^2 \tag{3}$$

is conserved, and is the center-of-mass energy squared of the system. It is the energy available to create new particles, or probing the properties of particles.

2.3 Top Quarks

The top quark is the third generation up-type quark in the SM, with a charge of $+2/3e$, and the greatest mass of all the known elementary particles. Top quark has a weak two-body decay and its decay can be analyzed from the Cabbibo-Kaboyashi-Maskawa matrix (CKM). The diagonal part of the CKM matrix, shows quarks transition predominantly within their own family, with very little deviation from unity. This is especially true for the top quark, where top quarks decays into bottom quarks and W bosons 99.8% of the time. Because the top quark decays as a free quark, we can use the polarization as an observable, because its spin will be preserved in the decay product.

There are two primary mechanisms for the production of top quarks at the LHC, a single top via weak interactions, or the pair production via the strong force. The pair production of top quark is a QCD effect, which takes place by gluon fusion $gg \to t\bar{t}$ and quark-antiquark annihilation $q\bar{q} \to t\bar{t}$. The branching fraction of each of the pair production processes, is related to the center-of-mass energy, for which gluon fusion dominates at the LHC at about 86% of the production.

2.4 Coupling of W^+tb

The leptonic decay of the Wboson, can decay into either of the three leptonic families, with nearly equal branching ratios. The τ lepton is also very

unstable and has too short a lifetime, so it does not get tagged in this paper. τ-particles that decay by weak interaction into electrons, $\tau^+ \to e^+\nu_e$, or muons, $\tau^+ \to \mu^+\nu_\mu$, are tagged as part of the single lepton channel.

The Wboson couples only to left-handed fermions, or right handed anti-fermions, giving Wtb vortex a (V-A) structure. In the Standard Model we expect that the Wboson and $b$quark from top decay, arrange such that chiral structure of the couple vertex is fulfilled. Because of parity violation, the events with positive helicity (right polarized) gets suppressed, while events with negative (left polarized) and longitudinal helicity dominates.

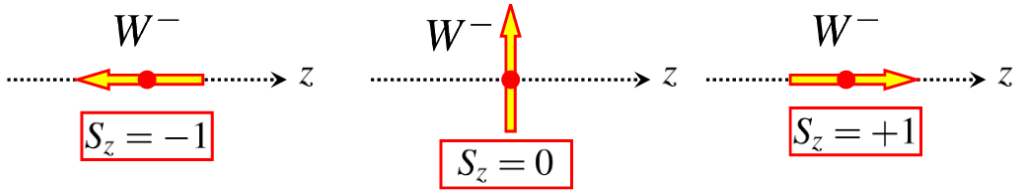

Figure 2: The figure illustrates W-boson with negative, zero and positive helicity, corresponding to a left, longitudinal and right handed polarization. The right handed polarization will be heavily suppressed because of the (V-A) structure of the Wtb vertex.

The fraction of; longitudinally F_0, left F_L or right F_R polarized $W-$bosons which are produced from top quark decay, we refer to as helicity fractions. In the Standard Model we can determine these fractions with quantum chromo dynamics, in next to next to leading order (NNLO) calculations to be $F_0 = 0.687 \pm 0.005$, $F_L = 0.311 \pm 0.005$ and $F_R = 0.0017 \pm 0.0001$[3]. The experimental method to extract these fractions is by studying the angular decay distribution of the leptonic decay products of the top quark. The angular distribution is given by:

$$\frac{1}{\Gamma}\frac{\mathrm{d}\Gamma}{\mathrm{d}\cos\theta^*} = \frac{3}{8}(1-\cos\theta^*)^2 F_L + \frac{3}{4}\sin^2\theta^* F_0 + \frac{3}{8}(1+\cos\theta^*)^2 F_R. \qquad (4)$$

Where θ^* is the helicity angle, which is defined as the angle between the decayed lepton momentum direction, and the reversible momentum direction of the b-quark decay from the same top quark, viewed from a reference frame with W at rest[8]. From the 4-vectors of the lepton and b-jet, we can find the $\cos\theta^*$ from the following expression:

$$\frac{2M_{eb}^2}{m_t^2 - M_W^2} - 1, \qquad (5)$$

here p_l and p_b are the four momentum vectors of the lepton and the bottom quark respectively. M_{lb} is the invariant mass of the lepton and bottom quark system. The dependence is shown in Fig. 3 for the three distribution seperately, and for the SM, with the above mentioned NNLO helicity fractions.

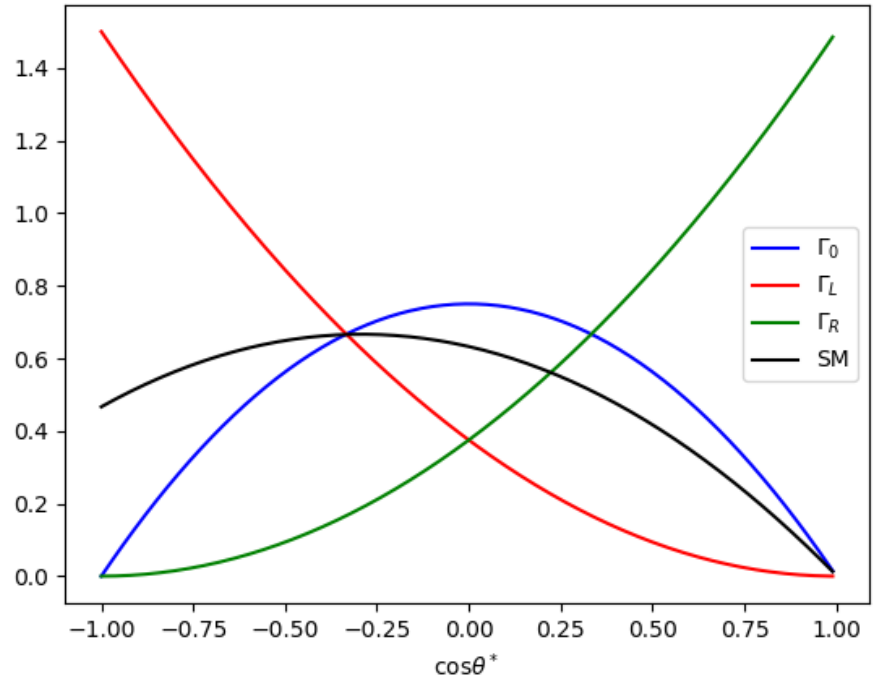

Figure 3: The predicted $\cos\theta^*$ angular distribution for helicity fractions. The distributions for F_0, F_L and F_R are normalized, and are given by the blue, red and green line respectively. The black line is the sum of the three contributions, but with helicity fractions given according to SM predictions.

Another approach to obtaining the polarization states the W-bosons, is done by counting the number of events with a specific $\cos\theta^*$, then use angular asymmetries, A_-, and A_+, defined as

$$A_\pm = \frac{N(\cos\theta^* > z) - N(\cos\theta^* < z)}{N(\cos\theta^* > z) + N(\cos\theta^* < z)}, \tag{6}$$

with $z = \pm(2^{2/3} - 1)$, to choose asymmetries involving only dependence on F_0 and F_L for A_+, or F_0 and F_R for A_-. The helicity fractions for the W

boson, can then be obtained by,

$$F_R = \frac{1}{1-\beta} + \frac{A_- - \beta A_+}{3\beta(1-\beta^2)}, \tag{7}$$

$$F_L = \frac{1}{1-\beta} + \frac{A_+ - \beta A_-}{3\beta(1-\beta^2)}, \tag{8}$$

$$F_0 = \frac{1+\beta}{1-\beta} + \frac{A_+ - A_-}{3\beta(1-\beta)}, \tag{9}$$

where $\beta = 2^{1/3} - 1$. The values for angular asymmetries is calculated in SM NNLO as $A_+ = 0.537 \pm 0.004$ and $A_- = -0.0841 \pm 0.006$.

3 Apparatus

3.1 LHC

In the Large Hadron Collider, top quarks are mainly produced through violent collisions of protons, causing gluon-gluon fusion, which produces top, anti-top pairs $gg \to t\bar{t}$. The data used in this paper, is from the 2016 run at LHC, with a centre-of-mass energy of $\sqrt{s} = 13$TeV, which corresponds to an integrated luminosity of 10 fb^{-1}[12]. At these energies, the protons are accelerated close to the speed of light before their collisions in the ATLAS detector.

This process starts, when protons are generated from an ion source in the linear accelerator, LINAC2, then gets injected into the LHC, through a series of smaller synchrotron accelerators, Proton Syncrotron Booster (PSB), Proton Syncrotron (PS) and Super Protron Synhrotron (SPS)[4, p. 135]. The LHC receives bunches from another SPS, containing a lot of protons in each bunch, effectively increasing the cross-sectional area for collisions to occur. In order to prevent energy loss due to synchrotron radiation, the LHC was built to be the largest particle accelerator in the world, which has allowed it to reach higher energies than other accelerators. At these energies, more events happen inside the detector, described by the following equation:

$$N = \sigma \int L \mathrm{d}t, \tag{10}$$

where N is the number of expected events, σ is the cross-sectional area of the events, and $\int L\mathrm{d}t$ is the integrated luminosity.

3.2 ATLAS

The ATLAS detector consists of multiple primary components, each with their own subcomponents or subsections.

3.2.1 The Inner Detector

The purpose of this component is to measure charge and momentum, including it's direction, of the detected particle. It consists of three subcomponents.

Pixel Detector The pixel detector consists of approximately 92 million electronic channels. It's used for identification and reconstruction of secondary vertices from decay of particles containing a b-quark or for b-tagging jets. The pixel detector covers pseudorapidity range $|\eta| < 2.5$

Semiconductor Tracker The Semiconductor tracker is a silicon microstrip tracker consisting of 4088 two-sided modules and over 6 million readout strips. These readout strips are distributed every 80μm which allows recording of the position of charged particles to an accuracy of 17μm

Transition Radiation Tracker. The transition radiation tracker is a drift tube tracker which consists of a straw of 4mm diameter and 0.03mm diameter tungsten wire coated with 0.5-0.7mm gold. The tube is filled with a gas mixture of Xe, CO_2 and O_2. When charged particles travel through the tube the gas gets ionized which frees electrons that move to the gold wire. The negative charge measured on the wire can be used to distinguish which charged particle ionzed the gas.

3.2.2 Calorimeter

This component will stop particles moving through while measuring the energy they lose by being stopped. The Calorimeter can not stop muons and neutrinos. Region up to $|\eta| < 4.9$ is covered.

Liquid Argon Calorimeter

Tile Hadronic Calorimeter Measures hadrons

3.2.3 Muon Spectrometer

This detects the muons, which have passed through the calorimeter and inner detector, and measures their momenta.

Thin Gap Chambers

Resistive Plate Chambers

Monitored Drift Tubes

Cathode Strip Chambers

3.2.4 Magnet System

This system bends the path of the particles, such that their track stays within the confines of the detector.

Central Solenoid Magnet

Barrel Toroid

End-cap Toroids

3.2.5 Data Collection

The detector generates 60 terabytes of data per second from the 1.7 billion collisions taking place in the detector in that time frame. Therefore, The ATLAS Detector has a hardware trigger system which helps selectively save only data in which a particle has been detected.

4 Monte Carlo Simulation

Monte Carlo (MC) simulation was used to model the signal and background processes expected at the LHC, for the 13 TeV Atlas Open Data used for this report. This process follows four steps, starting with an event generation which uses a MC generator to mimic the initial pp collision. In the second step, detector simulation, the geometry of the ATLAS detector and its material properties gets simulated. As part of the digitisation step, the previous step is followed by simulating the responding signals in read-out data written in a format compatible with real output of the detector. Finally these data can be used to reconstruct the collisions, particle trajectories and subsequent products.

In The 13 TeV ATLAS Open Data set, there are several SM processes which are modelled using MC simulations. For the purpose of this report, the MC simulations on top-quark-pair production was used alongside real data taken from the detector, to compare theory with real data.

5 Data Analysis

5.1 Event Selection

In order to identify the top-quark-pair production, several cuts in the data were implemented. The criteria are as follows

- Only one electron or muon in the final state with $p_T > 30\text{GeV}$
- Missing transverse momentum $E_T^{miss} > 30\text{GeV}$
- Transverse mass of the W-boson $M_T^W > 30\text{GeV}$
- At least four jets with $p_T > 30\text{GeV}$, with exactly two of these being b-tagged
- Electrons are required to have $|\eta| > 2.47$ aside from $1.37 < |\eta| < 1.52$
- Muons are limited by $|\eta| > 2.50$

where η describes angle between the particle and the beam axis given by

$$\eta = -\ln\left(\tan\left(\frac{\theta}{2}\right)\right) \tag{11}$$

5.1.1 B-tagging

To study the Wtb structure, a mechanism to identify the b-jets from the other detected jets is required. First the jets are detected, b-hadrons, c-hadrons or light-flavour jets, then their trajectories (tracks) are reconstructed in the inner detector. Once a jet has been found, the jets contining b-hadrons are then identified by a combination of three distinct algorithms. Hadrons containing b-quarks have a long enough lifetime to fly a measurable distance before it decays, and can be exploted to built lifetime-based tagging algorithms. The impact parameter based algorithm, IP3D, uses transverse and longitudinal impact parameter significances of each track within a jet, the SV reconstructs the secondary vertex within the jet and decay chain multi-vertex algorithm (JetFitter) reconstructs the full b-hadron decay chain.

To better discriminate between jets, a Boosted Decision Tree (BDT) algorithm called MV2c10, which uses the Root Toolkit for Multivariate Data Analysis (TMVA), is used to make cuts that discards most of the background components, the c- and light-flavoured jets. For this report, a b-jet efficiency rate of 70% is used, which corresponds to a BDT cut value of 0.8244. This efficiency rate originates from samples of simulated $t\bar{t}$ events with a c- and light-jet rejection factor of nearly 400[10]. At these cuts, most of the c-jets and light-flavoured jets gets rejected, while still maintaining most of the b-jet data.

5.2 Histograms from the ATLAS data

After we have identified top-quark pair production we know that only one lepton should be present in the event. This means that we can use the first lepton in the event as the leading lepton. This lepton, however, can be either a electron or a muon. Using this information we can construct the Lorentz vector for the lepton, and from this we can plot the transverse energy. To calculate the transverse energy we are using the builtin ROOT `TLorentzVector` member function `Et()`. That function is effectively defined as

$$E_t = p_t \frac{\sqrt{p_y^2 + p_x^2}}{\sqrt{p_z^2 + p_y^2 + p_x^2}} \tag{12}$$

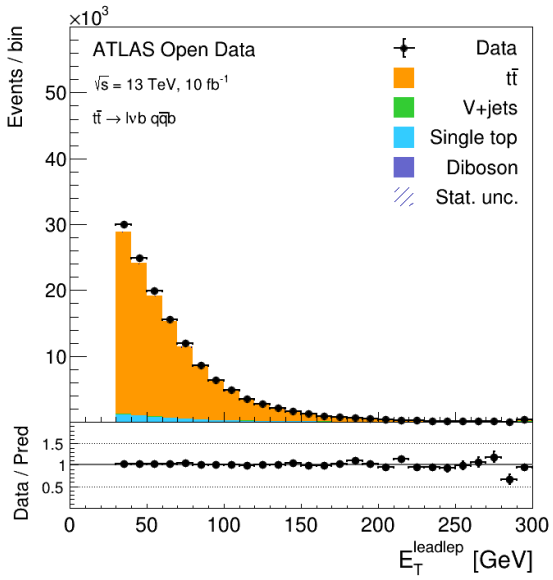

Figure 4: Lead lepton transverse energy for both single-electron and single-muon channel.

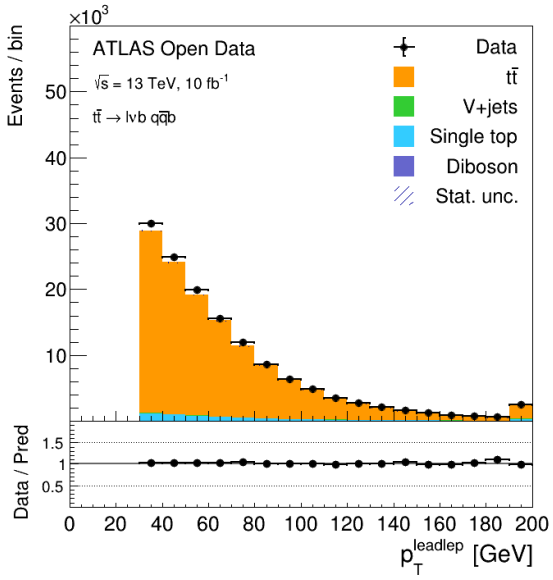

Figure 5: Lead lepton transverse momentum for both single-electron and single-muon channel.

In the given data we are directly given the missing transverse energy, which we can then immediately plot if the given event satisfies all the criteria

given in subsection 5.1. It is worth noting that it is given in the unit MeV, and all we have to do is simply convert to GeV, for a more manageable unit in the plot.

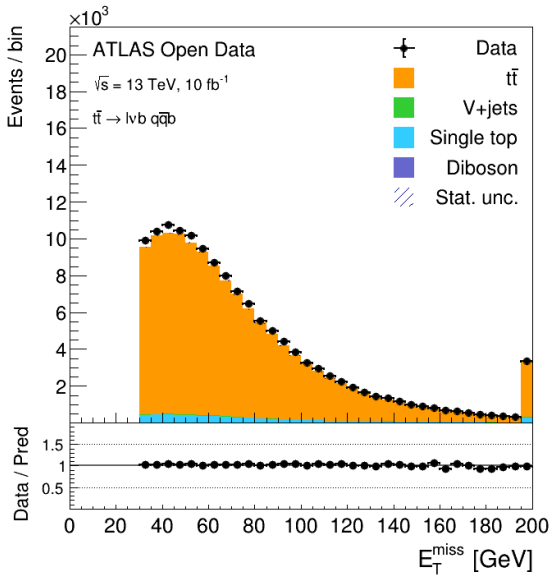

Figure 6: Missing transverse energy for both single-electron and single-muon channel.

We are also given transverse momentum of jets in the event. The jets in the event are ordered and we can therefore get information about the leading jet by accessing the first one.

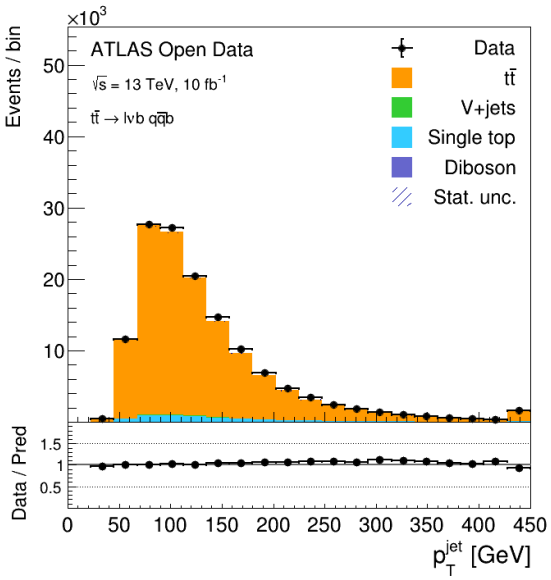

Figure 7: Lead jet transverse momentum for both single-electron and single-muon channel.

5.3 $\cos\theta^*$ reconstruction

From the data we can reconstruct $\cos\theta^*$ using equation (5).

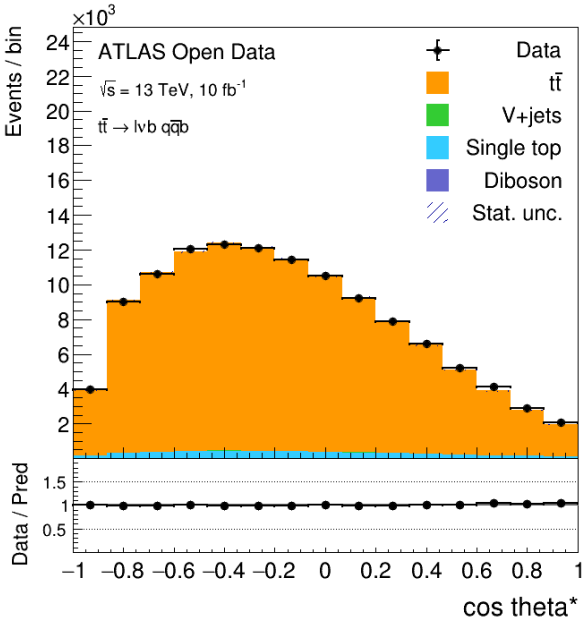

Figure 8: Reconstructed $\cos\theta^*$ from ATLAS data.

5.4 Delphes data

Using delphes we can at least verify that the generated data at least matches the theoretical analytical functions plotted in figure 3 as a sanity check. Using the same information, as we would get in the ATLAS data, we can use the same criteria from subsection 5.1 to isolate the equivalent usable data, as we would get from the ATLAS detector, in the delphes data. We can now fit the resulting histograms in a linear combination to the histogram from the ATLAS data.

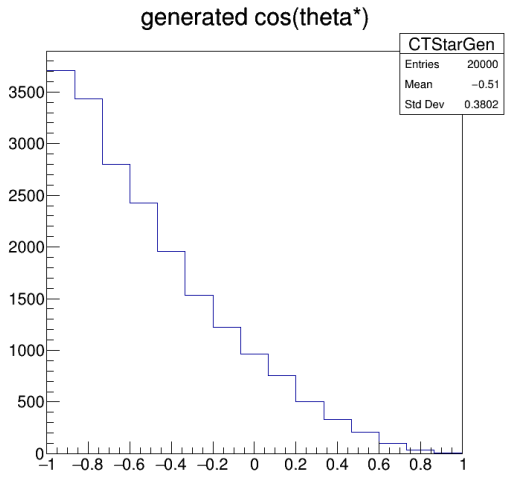

(a) Lorem ipsum

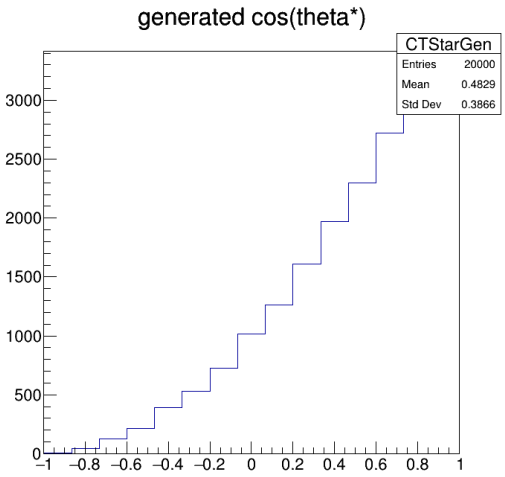

(b) Lorem ipsum, lorem ipsum,Lorem ipsum, lorem ipsum,Lorem ipsum

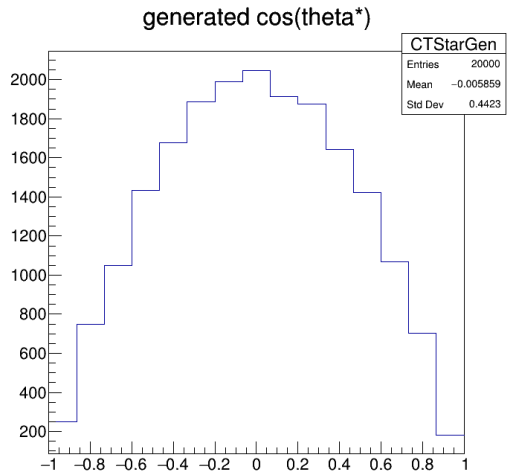

(c) Lorem ipsum, lorem ipsum,Lorem ipsum, lorem ipsum,Lorem ipsum

Figure 9: Caption place holder

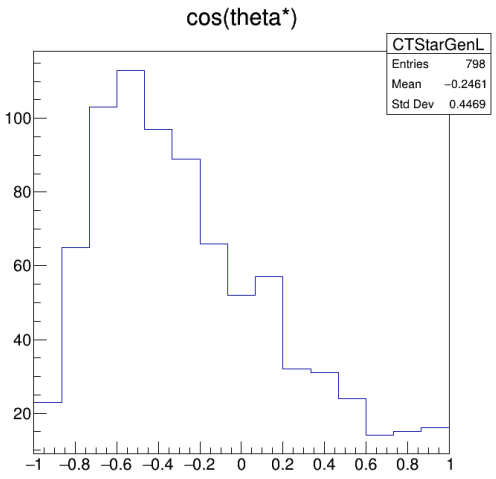

(a) Lorem ipsum

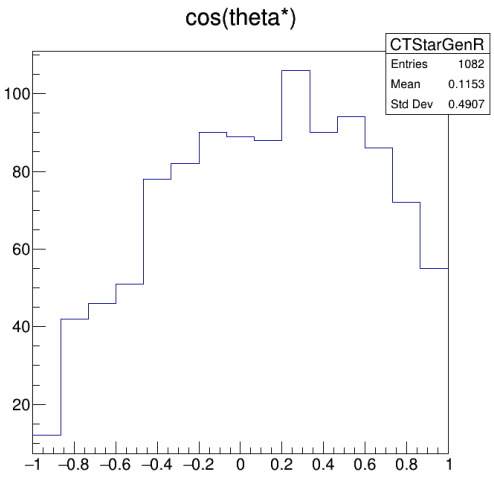

(b) Lorem ipsum, lorem ipsum,Lorem ipsum, lorem ipsum,Lorem ipsum

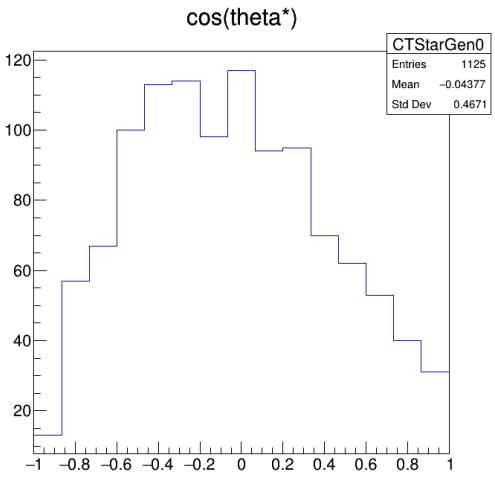

(c) Lorem ipsum, lorem ipsum,Lorem ipsum, lorem ipsum,Lorem ipsum

Figure 10: Caption place holder

5.5 Fitting to atlas data

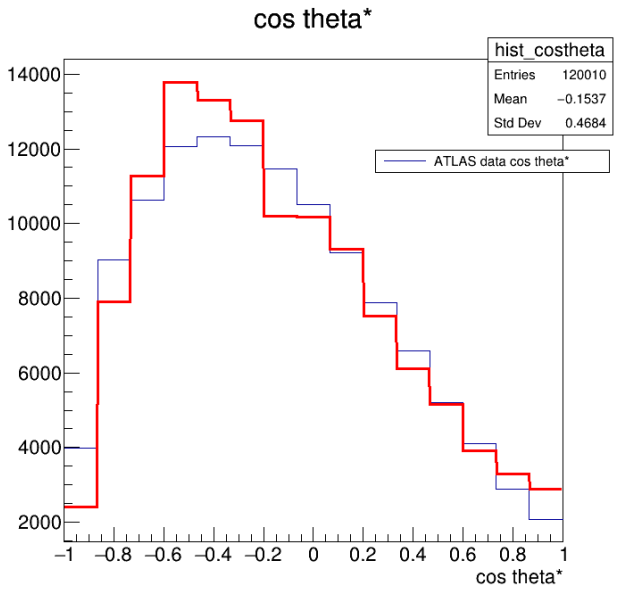

Figure 11: Reconstructed Delphes $\cos\theta^*$ fitted to the $\cos\theta^*$ from ATLAS data.

```
FCN=954.777 FROM MIGRAD    STATUS=CONVERGED   217 CALLS   218 TOTAL
          EDM=3.15154e-10    STRATEGY= 1      ERROR MATRIX ACCURATE
 NO. PARAMETER VALUE          ERROR          STEP SIZE  FIRST DERIVATIVE
  1  F_0       4.00289e+01   1.28234e+00   4.79954e-03  -4.35846e-05
  2  F_L       2.79292e+01   4.50791e-01   3.37816e-03  -6.07790e-05
  3  F_R       2.28996e-01   4.03043e-01   2.22299e-03  -4.81292e-05
                             ERR DEF= 0.5
```

5.6 The Code

5.6.1 ROOT

5.7 Results

6 Discussion

Due to the limitations of the released 13 TeV Open Datasets, it was not possible to analyse the helicity fractions angular distribution through that data, which lead to the utilization of Delphes. The deviation between the predicted

SM values for the helicity fraction, and the value obtained through the fitting, is possible the result of systematic errors in attempting to fit Delphes simulated spin orientation, to the data obtained from the LHC Open ATLAS run in 2016. Since Delphes runs a fast-simulation, it is not designed to be used in parallel with data taken from advanced detector studies. This analysis consequently serves as a test for this novel approach of combining Delphes simulations with data taken from ATLAS detector. While similar cuts was attempted to be implemented on the Delphes' truth-information, due to the absence of the b-tagging MV2c10 algorithm in Delphes, cuts were made using 80% efficiency instead.

The reconstructed $\cos\theta^*$ had significant entries in overflow. Attempts using the theoretical $\cos\theta^*$, rather than the approximation, as seen in Eq. 5, but no visible differences appeared, and the overflow remained. This overflow was ignored in the fitting process, as only data remaining within the physically possible range from -1 to 1, was considered in the analysis. The Delphes data for the helicity destributions, had substantially less overflow, than data from OpenATLAS, which also motived the decision to only fit within the parameter -1 to 1.

7 Conclusion

References

[1] S. Abachi et al. "Observation of the Top Quark". In: *Physical Review Letters* 74.14 (Apr. 1995), pp. 2632–2637. ISSN: 1079-7114. DOI: 10.1103/physrevlett.74.2632. URL: http://dx.doi.org/10.1103/PhysRevLett.74.2632.

[2] F. Abe et al. "Observation of Top Quark Production inp¯pCollisions with the Collider Detector at Fermilab". In: *Physical Review Letters* 74.14 (Apr. 1995), pp. 2626–2631. ISSN: 1079-7114. DOI: 10.1103/physrevlett.74.2626. URL: http://dx.doi.org/10.1103/PhysRevLett.74.2626.

[3] Andrzej Czarnecki, Jürgen G. Körner, and Jan H. Piclum. "Helicity fractions ofWbosons from top quark decays at next-to-next-to-leading order in QCD". In: *Physical Review D* 81.11 (June 2010). ISSN: 1550-2368. DOI: 10.1103/physrevd.81.111503. URL: http://dx.doi.org/10.1103/PhysRevD.81.111503.

[4] Lyndon Evans and Philip Bryant. "LHC Machine". In: *Journal of Instrumentation* 3.08 (Aug. 2008), S08001–S08001. DOI: 10.1088/1748-0221/3/08/s08001. URL: https://doi.org/10.1088/1748-0221/3/08/s08001.

[5] J. de Favereau et al. "DELPHES 3: a modular framework for fast simulation of a generic collider experiment". In: *Journal of High Energy Physics* 2014.2 (Feb. 2014). ISSN: 1029-8479. DOI: 10.1007/jhep02(2014)057. URL: http://dx.doi.org/10.1007/JHEP02(2014)057.

[6] H. Fritzsch, M. Gell-Mann, and H. Leutwyler. "Advantages of the color octet gluon picture". In: *Physics Letters B* 47.4 (1973), pp. 365–368. ISSN: 0370-2693. DOI: https://doi.org/10.1016/0370-2693(73)90625-4. URL: https://www.sciencedirect.com/science/article/pii/0370269373906254.

[7] M. Gell-Mann. "A schematic model of baryons and mesons". In: *Physics Letters* 8.3 (1964), pp. 214–215. ISSN: 0031-9163. DOI: https://doi.org/10.1016/S0031-9163(64)92001-3. URL: https://www.sciencedirect.com/science/article/pii/S0031916364920013.

[8] G. L. Kane, G. A. Ladinsky, and C. -P. Yuan. "Using the top quark for testing standard-model polarization and CP predictions". In: *Phys. Rev. D* 45 (1 Jan. 1992), pp. 124–141. DOI: 10.1103/PhysRevD.45.124. URL: https://link.aps.org/doi/10.1103/PhysRevD.45.124.

[9] Emmy Noether. "Invariant variation problems". In: *Transport Theory and Statistical Physics* 1.3 (Jan. 1971), pp. 186–207. ISSN: 1532-2424. DOI: 10.1080/00411457108231446. URL: http://dx.doi.org/10.1080/00411457108231446.

[10] *Optimisation of the ATLAS b-tagging performance for the 2016 LHC Run*. Tech. rep. All figures including auxiliary figures are available at https://atlas.web.cern.ch/Atlas/GROUPS/PHYSICS/PUBNOTES/ATL-PHYS-PUB-2016-012. Geneva: CERN, June 2016. URL: https://cds.cern.ch/record/2160731.

[11] Bogdan Povh et al. *Particles and Nuclei*. Springer Berlin Heidelberg, 2015. DOI: 10.1007/978-3-662-46321-5. URL: https://doi.org/10.1007/978-3-662-46321-5.

[12] *Review of the 13 TeV ATLAS Open Data release*. Tech. rep. ATL-OREACH-PUB-2020-001. Geneva: CERN, Jan. 2020. URL: https://cds.cern.ch/record/2707171.

[13] C. S. Wu et al. “Experimental Test of Parity Conservation in Beta Decay”. In: *Phys. Rev.* 105 (4 Feb. 1957), pp. 1413–1415. DOI: 10.1103/PhysRev.105.1413. URL: https://link.aps.org/doi/10.1103/PhysRev.105.1413.

[14] A. Zee. *Group Theory in a Nutshell for Physicists*. Princeton University Press, Mar. 2016. ISBN: 0691162697. URL: https://www.xarg.org/ref/a/0691162697/.